Article type : Technical Paper

Hydroclimatology of the Mississippi River Basin

Gregory J. McCabe and David M. Wolock

Integrated Modeling and Prediction Division (**McCabe**), U.S. Geological Survey, Denver, Colorado USA; and Integrated Modeling and Prediction Division (**Wolock**), U.S. Geological Survey Lawrence, Kansas, USA (Correspondence to McCabe: gmccabe@usgs.gov).

Research Impact Statement: This study provides a baseline understanding of the hydroclimatology of the Mississippi River basin (MRB) and can be used to guide the selection of regions within the MRB for targeted analyses.

ABSTRACT: Model estimated monthly water balance components (i.e. potential evapotranspiration, actual evapotranspiration, and runoff (R)) for 848 U.S. Geological Survey 8-digit hydrologic units located in the Mississippi River basin (MRB) are used to examine the temporal and spatial variability of the MRB water balance for water years 1901 through 2014. Results indicate the MRB can be divided into 9 sub-regions with similar temporal variability in R. The water balance analyses indicated ~79 percent of total water-year MRB runoff is generated by 4 of the 9 sub-regions and most of the R in the basin is derived from surplus (S) water during

the months of December through May. Furthermore, the analyses showed temporal variability in S is largely controlled by the occurrence of negative atmospheric pressure anomalies over the western U.S. and positive atmospheric pressure anomalies over the eastern U.S. coast. This combination of atmospheric pressure anomalies results in an anomalous flow of moist air from the Gulf of Mexico into the MRB. In the context of paleo-climate reconstructions of the Palmer Drought Severity Index, since about 1900 the MRB has experienced wetter conditions than were experienced during the previous 500 years.

(**KEYWORDS:** hydroclimatology; Mississippi River; water balance; hydrology.)

INTRODUCTION

The Mississippi River basin (MRB) drains nearly two thirds of the conterminous United States (U.S.) and is an important water supply for agricultural and urban areas; the MRB also serves as an important waterway for U.S. industry. In addition, the MRB is a major source of nutrient over-enrichment to the Gulf of Mexico (primarily from fertilizer and manure) (Goolsby et al., 1999; Rabalais et al., 1999). The excess nutrients delivered to the Gulf of Mexico from the MRB result in increased algal growth and, subsequently, eutrophication (Rabalais et al., 1999), which can deplete oxygen levels resulting in hypoxia. Many aquatic species cannot survive in the hypoxic zone in the Gulf of Mexico, which is co-located with important commercial and recreational fisheries (Rabalais et al., 1999). Although the MRB is one of the largest and most important rivers in the U.S. there have been only a few comprehensive analyses of the water balance of this important river basin.

One previous study of MRB hydroclimate by Baldwin and Lall (1999) examined variability and trends in the seasonality of upper MRB streamflow and presented evidence of changes in both the timing and amplitude of seasonal and annual MRB flow extremes. Milly and Dunne (2001) also examined temporal variability and trends of MRB hydroclimate by examining surface water and energy balances in the MRB. Milly and Dunne (2001) reported a positive trend in MRB evaporation during 1948 through 1997 that was primarily associated with increases in precipitation (P) and secondarily with human water use. Milly and Dunne (2001) also suggested that the increase in P in the MRB was related to a positive trend in the North Atlantic Oscillation.

Massei et al. (2011) used wavelet analysis to examine hydroclimate variability in the MRB for the period 1934 to 1998 and showed that a major shift in MRB hydroclimate occurred around 1970. This shift was characterized by an 8 to 16-year mode of variability in the Upper Mississippi and Missouri Rivers and a 3 to 6-year mode of variability for most MRB tributaries. In general, the dominant modes of inter-annual to multi-annual streamflow variability were found to be in the 2 to 4-year, 4 to 8-year and 10 to 16-year periods, which indicates an influence of the El Nino Southern Oscillation. Massei et al. (2011) found that variability in multi-annual frequencies explained from 6% to 26% of streamflow variance across the MRB, while higher frequencies of 2 to 3 weeks explained from 1% to 6% of streamflow variability across the MRB. In general, however, variability on annual time scales explained the largest amount of variability in MRB streamflow accounting for 19% to 48% of the total variation. Massei et al. (2011) also reported that all streamflow time series exhibited statistically significant positive trends.

In a related study, Qian et al. (2007) examined trends in surface water and energy budget components for the MRB for the period 1948 to 2004 using a combination of observations and simulations from the Community Land Model version 3 (CLM3). The model analyses indicated that increases in MRB-averaged precipitation were accompanied by increases in both runoff and evapotranspiration. Additionally, a decrease of MRB net shortwave radiation largely driven by increases in cloudiness was accompanied by decreases in both net longwave radiation and sensible heat flux, whereas latent heat flux increased due to wetter soils. These results confirmed observations that evapotranspiration increased in the MRB from 1948 to 2004. Qian et al. (2007) also reported that precipitation trends were the primary control of trends in evapotranspiration, while trends in temperature and solar radiation had only a small effect.

Frans et al. (2013) used a macroscale hydrology model to examine the effects of land use/land cover changes and climate variability on temporal changes in MRB hydroclimate for 1918 through 2007. Frans et al. (2013) concluded that climate change was the primary factor driving MRB runoff changes.

Recently, Wise et al. (2018) completed a comprehensive study of the hydroclimate of the Missouri River basin (a major tributary of the MRB). Wise et al. (2018) analyzed observed and modeled hydroclimatic data in the Missouri River basin and reported that 72% of Missouri River runoff is generated by two regions: (1) the headwaters in the upper Missouri River basin, and (2) the lowest portion of the basin near the mouth. Wise et al. (2018) also reported that a long-term negative trend (for years 1912 through 2011) in upper Missouri River basin flows and a decrease in upper Missouri River snow versus rain fractions (for years 1936 through 2011) were associated with warming spring temperatures. Wise et al. (2018) concluded that these hydroclimatic changes in the upper Missouri River indicate that the upper Missouri River basin may not continue to reliably provide flow contributions to the lower Missouri River basin in the future.

Although there have been analyses of the variability and trends in several water balance components for the MRB (e.g. precipitation, evapotranspiration, streamflow), there has not been a comprehensive and up-to-date evaluation of the spatial and temporal variability of water balance components for the MRB. The objectives of this research are to (1) characterize the spatial and temporal variability of water balance components in the MRB, (2) identify which sub-regions of the MRB, and during what times of the year, contribute the most to total MRB runoff, and (3) identify atmospheric circulation patterns associated with MRB runoff variability. This study will provide a baseline to which future analyses of variability and trends in MRB hydroclimatic variables can be compared.

DATA AND METHODS

Climate Data and Water Balance Simulations

Monthly precipitation (P) and temperature (T) data were obtained from the parameter regression on independent slopes model (PRISM) (PRISM Climate Group, Oregon State University, http://www.prism.oregonstate.edu; Daly et al. 2008). These data are provided on a 4-kilometer (km) resolution for grid cells across the conterminous U.S. (CONUS) for the period January 1895 until present. These data were spatially aggregated to provide monthly total P and mean monthly T for the 848 U.S. Geological Survey 8-digit hydrologic units (HUs) in the MRB (Figure 1). The aggregation of the PRISM data to the HU scale reduced the number of data points and allows for analyses to be more computationally efficient. The monthly T and P data aggregated to the HUs subsequently were used as input to a monthly water balance model (WB model) to compute monthly potential evapotranspiration (PET), actual evapotranspiration (AET), surplus (S), and runoff (R) for each HU in the MRB (McCabe and Wolock, 2011). S is the amount of water in a month that exceeds the water needed to meet the PET demand and bring soil moisture storage to capacity; S is the water that eventually becomes runoff.

Soil-moisture storage capacity for each HU was computed using the available water-capacity values from the State Soil Geographic Data Base (STATSGO) dataset and by assuming a 1-meter rooting depth (STATSGO soil data are available at https://www.nrcs.usda.gov/wps/portal/nrcs/detail/soils/survey/geo/?cid=nrcs142p2_053629; U.S. Department of Agriculture, 1991).

The WB model has been evaluated in several previous studies (McCabe and Wolock, 2008; McCabe and Wolock, 2011). McCabe and Wolock (2011) compared WB model estimated (WB-estimated) R and measured R for 735 basins across the conterminous U.S. Comparison of measured and estimated monthly runoff indicated that the WB model reliably simulated the temporal variability of monthly runoff for most of the stream gauges. The distribution of correlation values between WB-estimated monthly R and measured monthly R for the 735 stream gauges had a median value of 0.78, with a 25th percentile value of 0.61 and a 75th percentile value of 0.87 (these correlations are statistically significant at a 99% confidence level ($p < 0.01$)). Additionally, the mean bias for the 735 stream gauges was 1 millimeter (mm), with a 25th percentile of -3 mm and a 75th percentile of 5 mm.

Figure 2 illustrates a comparison of measured and WB-estimated water-year R for the MRB; a water year is the period from October 1 through September 30. The correlation coefficient (r) between the time series is 0.95 ($p < 0.01$), with a bias (mean WB-estimated R minus mean measured R) of 7.2 mm (which is 3.3% of mean water-year measured R). We also performed comparisons of measured water-year R with WB-estimated water-year R for 10 sites within the MRB for the period 1955 through 2015. The sites were selected from a dataset compiled by Falcone et al. (2010) that includes stream gauges across the CONUS that are minimally affected by anthropogenic influences (e.g. dams, diversions, withdrawals). For most of the sites (7 of 10) examined, the correlation coefficient between measured and WB-estimated R is above 0.85 ($p < 0.01$) (Figure 3). Only for the sites with low runoff (i.e. sites 1 and 3) are the correlation coefficients below 0.85; however, even for these sites the correlation coefficients between measured and WB-estimated R are statistically significant at $p < 0.01$.

Previous verifications of the WB model and the comparisons between measured and WB-estimated R presented here indicate that the WB model reliably simulates runoff for the MRB. Given that on an annual basis, R = P - AET, the ability of the WB model to estimate R implies that the model also reliably estimates annual AET (McCabe and Wolock, 2013). A benefit of using the WB model is that R can be estimated back to the beginning of the 20th century. Additionally, by using the WB model, we also can examine time series of other water balance components such as PET and AET.

The PRISM T and P data begin in 1895; however, the first few years (i.e. 1895 through 1900) of the WB model simulations are not analyzed so that the effects of prescribed initial conditions are minimized. Thus, for the analyses presented in this study, WB model simulations for water years 1901 through 2014 are used. The WB model is initialized with soil moisture storage at capacity, snow storage equal to zero, and S equal to zero.

The monthly water balance estimates of PET, AET, S and R for the PRISM 4-km grid cells for the CONUS are available at https://doi.org/10.5066/F71V5CWN (Wolock and McCabe, 2018).

Figure 4a illustrates a map of mean elevation (in meters (m)) for each HU in the MRB. Elevations for the HUs range from 2 m near the mouth of the MRB to 4282 m along the western edge of the basin (on the eastern side of the Rocky Mountains). Mean annual T is highest in the southernmost locations (highest T = 21^{o}C) and lowest in the northwestern part of the MRB (lowest mean annual T = 0^{o}C) (Figure 4b). This spatial pattern is controlled by the latitude and elevations of the HUs. Mean annual P is highest (1690 mm) in the southeastern section of the MRB and lowest along the western margins of the MRB (230 mm) (Figure 4c). The high levels of P in the southeastern part of the MRB are due to the large influx of moisture from the Gulf of Mexico into this region. Because the spatial patterns of both T and P have a south to north gradient the Pearson correlation between these spatial patterns is $r=0.71$ ($p < 0.01$).

The spatial patterns of mean annual AET and R are strongly related to the spatial pattern of mean annual P (Figures 4d and 4e). The Pearson correlation between the patterns for AET and P is 0.93 ($p < 0.01$) and the correlation between the patterns of R and P is 0.95 ($p < 0.01$). However, since the spatial patterns of mean annual P and T both have a south to north gradient, the correlation between the spatial patterns of AET and R with T also are strongly positive, with the correlation between the AET and T patterns equal to 0.80 ($p < 0.01$) and the correlation between the R and T patterns equal to 0.54 ($p < 0.01$). For the HUs in the MRB mean annual AET ranges from 221 mm to 1060 mm, and mean annual R ranges from 9 mm to 1264 mm.

Data Reduction

The 848 times series (one for each HU in the MRB) were grouped to more readily analyze and understand the temporal patterns in the components of the water balance. This was achieved with a hierarchical cluster analysis on the time series of water-year R for each of the 848 HUs for water years 1901 through 2014. For the clustering procedure we used a correlation-based approach to identify sub-regions within the MRB that share similar characteristics of inter-annual water-year R variability for 1901 through 2014. First, the water-year R time series at each HU was correlated with the water-year R time series for all other HUs. The HU that was correlated with the most other HUs (at $r \geq 0.71$, $p < 0.01$, and explained variance is ~ 50 percent) was removed from the original set of HUs along with the HUs that are significantly correlated with the selected HU; these HUs comprise the first group. The process is repeated with the remaining HUs to obtain the second and then subsequent groups. The initial classification process resulted in all the 848 HUs being assigned to 1 of 9 groups. To ensure that all HUs were assigned to the optimal group, water-year R values for each HU in each group were averaged to produce a sub-region mean. Each individual HU water-year R time series was then correlated with each sub-region mean time series to confirm membership in the appropriate sub-region group. The median correlation coefficients between each HU and the respective group mean time series ranged from 0.58 (sub-region 2) to 0.83 (sub-region 7). Sub-regions are shown in Figure 5.

In addition to computing mean water-year R for each of the 9 sub-regions, time series of mean P, PET, AET and S also were computed for each sub-region. Additionally, long-term (water years 1901 through 2014) mean monthly P, PET, AET, S, and R were computed for each sub-region to examine mean monthly water balances.

Additional Data

Other data used for analyses included monthly 500 hecto-Pascal (500 hPa) height anomalies for the region 180 degrees (°) west longitude to 0° longitude and 10° north latitude to 70° north latitude (these data are provided on a 2° by 2° grid). The monthly 500 hPa data for water years 1901-2014 were used to compute Pearson correlations (Helsel and Hirsch, 1992) between monthly 500 hPa height anomalies and time series of monthly S for the MRB to explore atmospheric pressure patterns associated with variability of S for the 9 sub-regions. Atmospheric pressure data for the 500 hPa level were selected for use in this study because the 500 hPa atmospheric pressure surface provides a useful representation of mid-tropospheric atmospheric circulation that influences seasonal surface weather variations. The monthly 500 hPa data were obtained from the 20th Century Reanalysis Project (https://www.esrl.noaa.gov/psd/data/20thC_Rean/; Compo et al., 2011).

RESULTS AND DISCUSSION

Mean Monthly Water Balances

Mean monthly water balance components (i.e. P, PET, AET, and R) are illustrated for each of the 9 sub-regions (Figure 6). In general, both P and PET are highest during the warm season months (i.e. April through September). Because P and PET are temporally in phase, a substantial fraction of P on an annual basis is evaporated and transpired (i.e. AET). The fraction of annual P that becomes AET ranges from 0.61 (sub-region 9) to 0.94 (sub-region 4) (Table 1).

For all sub-regions, PET generally exceeds P during the warm season months (Figure 6). Thus, during the warm season most P becomes AET and there is little S that can become R. For sub-regions 1, 2, and 4, PET is near or greater than P for almost all months of the year, and on an annual basis PET exceeds P (Table 1). Thus, there is little R generated during any month in sub-regions 1, 2, and 4. Additionally, for these three sub-regions the ratio of water-year (October through September total) AET to water-year P ranges from 0.85 (sub-region 1) to 0.94 (sub-region 4), and the runoff efficiency (water-year R/water-year P) ranges from 0.07 (sub-region 4) to 0.15 (sub-region 1) (Table 1).

For sub-regions 6 through 9, P exceeds PET during most months, particularly during the cool season (i.e. October through March) and on an annual basis (Figure 6). The excess of annual P compared with annual PET for these sub-regions results in R being generated primarily during the cool season (Figure 6). However, because P and PET are generally in phase in the MRB, the runoff efficiencies (water-year R/water-year P) even for these sub-regions are small ranging from 0.26 (sub-region 6) to 0.39 (sub-region 9) (Table 1). These runoff efficiencies indicate that less than 40% of annual P results in R even for the wettest sub-regions of the MRB.

Mean monthly water balance components for sub-regions 3 and 5 indicate that annual P exceeds annual PET by only a small amount (Figure 6, Table 1). For example, the ratio of annual PET to annual P for sub-regions 3 and 5 are 0.96 and 0.95, respectively (Table 1). Because annual P and annual PET are similar for these sub-regions, little R is generated for these two sub-regions and the runoff efficiencies are small (0.17 for sub-region 3 and 0.18 for sub-region 5) (Table 1).

The magnitude of R that occurs for each sub-region indicates that the largest amounts of R occur for the eastern-most sub-regions (Figure 7). A comparison of mean monthly R for each sub-region indicates that the highest R occurs for sub-regions 7, 8, and 9 for most months of the year, with R from sub-region 9 being the highest during all months. In contrast, the lowest R occurs in sub-regions 1, 2, and 4. It also is notable that the month of peak R generally occurs later in the calendar year for the northern sub-regions. This shift to later timing of peak R for the most northern sub-regions is related to the effects of snow melt on R timing.

Annual Water Balances

Examination of time series of water-year water balance components for each of the 9 sub-regions provides additional information regarding the relative magnitudes and inter-annual variability of the water balance components (Figure 8). Because PET exceeds P for sub-regions 1, 2, and 4, almost all P is evaporated or transpired, and AET is approximately equal to P consistently for water years 1901 through 2014; the net result is minimal R generated within these sub-regions. In contrast, for sub-regions 7 through 9, P has exceeded PET throughout water years 1901 through 2014 (Figure 8). Thus, for sub-regions 7 through 9, AET and PET are almost equal in magnitude, but significantly lower than P (especially for sub-regions 8 and 9), resulting in R being consistently generated from these sub-regions every year.

For sub-regions 3, 5, and 6, there are years when water-year P exceeds PET and other years when water-year P is less than PET. However, some R was generated in these sub-regions every year during water years 1901 through 2014 (Figure 8).

Figure 9 provides a comparison of 11-year moving average Z-scores of mean water-year P, PET, AET and R for each of the 9 sub-regions. The Z-scores were computed by

$$Z_i = \frac{(X_i - \overline{X})}{\sigma} \quad (1)$$

where Z_i is the Z-score for variable X and water-year i, X_i is the raw variable value for year i, $\overline{X}$ is the long-term variable mean, and σ is the long-term standard deviation. Time series of Z-scores makes it easier to compare time series for different variables and for different sub-regions because each time series has a mean of zero and a variance of one. The time series were smoothed with an 11-year moving average to remove high frequency variability from the time series.

Examination and comparison of the time series of smoothed Z-scores for the 9 sub-regions indicates substantial variability in the water balance components for each sub-region and between sub-regions (Figure 9). The negative Z-scores for P, AET, and R, and the positive Z-scores for PET between 1930 and 1940 reflect the effects of the 1930s drought that affected a large part of the CONUS.

The most notable feature of the smoothed P, AET, and R Z-scores are positive Z-scores for nearly all sub-regions beginning about 1970. The change from largely negative to largely positive P, AET, and R Z-scores near 1970 occurred for a large part of the Mississippi River basin (Figure 9). This apparent shift to wetter conditions in the MRB near 1970 coincides with an apparent shift in P and R for many locations across the eastern CONUS (McCabe and Wolock, 2002). The driving factor for the 1970s shift to wetter conditions is not completely clear; however, Milly and Dunne (2001) suggest that the shift could be attributed to a change to more frequent positive values of the North Atlantic Oscillation.

Contributions to Total Mississippi River Basin Runoff

The magnitude of R varies across the 9 sub-regions, and this spatial variability in R influences the contribution of R from each sub-region to total R for the MRB. The magnitude of the contribution from each sub-region to total MRB R also is affected by the size of the sub-region. On average, sub-regions 5, 7, 8, and 9 contribute ~79% of mean water-year MRB R, with sub-region 8 contributing the most (28%, Figure 9a). Sub-regions 1, 2, 3, and 4 on average contribute the least to mean water-year MRB R (Figure 10a).

On a mean monthly basis, sub-region 8 contributes the most to MRB R for most months (Figure 10b). During the cool season sub-regions 7, 8, and 9 are the largest contributors to MRB R; however, during the warm season sub-region 5 becomes one of the highest two contributors to total MRB R. Contributions to total mean monthly MRB R from sub-regions 1, 2, 3, 4, and 6 are generally below 10% for all months (Figure 10b). On a water-year basis, sub-region 8 and sub-region 7 are the largest contributors to total MRB R, with sub-region 8 being the largest contributor 77% of the time during water years 1901 through 2014. (Table 2). In contrast, on a water-year basis, sub-regions 2, 3, and 4 are the smallest contributors to total MRB R, with sub-region 2 being the smallest contributor 60% of the time (Table 2).

The mean monthly contributions of R from each sub-region to total mean monthly MRB R has implications for identifying the sources and types of pollutants that are washed into the MRB. Spatial and temporal variability in R have been shown to be a primary factor affecting the fluxes of nutrients from the MRB to the Gulf of Mexico (Goolsby et al., 1999). Based on the sub-region contributions to total MRB R identified in this study, R from sub-regions 7, 8, and 9 likely accounts for a substantial fraction of pollutants entering the MRB streamflow during most months of the year, but particularly during the cool season months. In contrast, sub-region 5 becomes a primary source of potential pollution to the MRB during the warm season. This result is especially important because sub-region 5 includes agriculturally intensive areas with high fertilizer and herbicide use (Goolsby et al., 1999).

Surplus and Climate Drivers

Surplus (S) is the water that is in excess of PET (the climatic demand for water) and water needed to bring soil-moisture-storage to capacity. This is the water that can eventually become R. The majority of S in the MRB is generated during cool season months (Figure 11), particularly from December through May when ~81% of S occurs on average. S during each of the months from December through May accounts for at least 10% of the annual S. Because December through May are the months on average when most S occurs, total S for December through May for each water year (1901 through 2014) was correlated with gridded mean December through May 500 hPa heights (for water years 1901 through 2014) to examine relations between variability in S and variability in atmospheric pressures.

Correlations between mean MRB S and 500 hPa heights for the months of December through May indicate similar patterns of correlations for each month (Figure 12). The pattern of negative and positive correlations with 500 hPa heights is indicative of the pattern of negative and positive atmospheric pressure (i.e. 500 hPa height) anomalies associated with positive anomalies of MRB S. The correlations indicate that anomalously positive MRB S is driven by negative atmospheric pressure anomalies over the western U.S. and positive atmospheric pressure anomalies over the eastern U.S. coast (Figure 12). The juxtaposition of these atmospheric pressure anomalies results in an anomalous southerly flow of moist air from the

Gulf of Mexico into the MRB, which results in increased P, increased S, and eventually increased R. This relation is consistent for all the months during December through May.

CONCLUSIONS

Using a hierarchical clustering procedure water-year R for 848 HUs in the MRB were grouped into 9 geographically coherent sub-regions. Water balance analyses for these sub-regions indicate that (1) ~79% of total water-year MRB R is contributed by 4 of the 9 sub-regions (i.e. sub-regions 5, 7, 8, and 9), all of which are located in the eastern-most part of the MRB, (2) most of the contributions to MRB R from these sub-regions occurs during the cool season months, although contributions of R from sub-region 5 are largest during the warm season, and (3) sub-region 8 contributes the most to total MRB water-year R 77% of the time, whereas sub-region 2 contributes the least to MRB water-year runoff 60% of the time. Given the sensitivity of nutrient fluxes in the MRB to variability in R, the timing and severity of Gulf of Mexico hypoxia is likely determined in large part by the hydroclimatic variability of the MRB.

An examination of time series of water balance variables for the 9 sub-regions indicates a change from largely negative to largely positive P, AET, and R Z-scores near 1970 for a large part of the MRB. This apparent change to wetter conditions in the MRB coincides with an apparent shift in P and R for many locations across the eastern CONUS (McCabe and Wolock, 2002) and may be related to a shift in the North Atlantic Oscillation to more positive values (Milly and Dunne, 2001).

Most R in the MRB is derived from S that occurs during December through May. Correlations between mean MRB S and 500 hPa heights for each month during December through May indicate that positive departures of S are associated with negative atmospheric pressure anomalies over the western U.S. and positive atmospheric pressure anomalies over the eastern U.S. coast. These atmospheric pressure anomalies result in an anomalous southerly flow of moist air from the Gulf of Mexico into the MRB, which results in increased P, increased S, and eventually increased R.

The results of this study provide a baseline understanding of the hydroclimatology of the MRB which can be used as a starting point for additional analyses. For instance, the effects of changes in climate (e.g. temperature and precipitation) on the hydroclimate of the MRB can be measured against the reference hydroclimate characterized in this study. Additionally, the baseline MRB hydroclimatology depicted in this study can be used to guide the selection of regions within the MRB for specific analyses. As an example, studies of climatic effects on the Gulf of Mexico hypoxic zone likely warrant focus on the variability and trends in the hydroclimate of MRB sub-regions 5 and 8 because these sub-regions are relatively large contributors to MRB R and are regions with a large amount of agriculture. Lastly, the hydroclimatic analysis of the MRB presented in this paper serves as a complement to the hydroclimatic analysis of the Missouri River basin (a major tributary of the MRB) presented by Wise et al. (2018).

ACKNOWLEDGEMENTS

Support for the Twentieth Century Reanalysis Project dataset is provided by the U.S. Department of Energy, Office of Science Innovative and Novel Computational Impact on Theory and Experiment (DOE INCITE) program, and Office of Biological and Environmental Research (BER), and by the National Oceanic and Atmospheric Administration Climate Program Office).

LITERATURE CITED

Baldwin, C.K., and U. Lall, 1999. “Seasonality of Streamflow: The Upper Mississippi River.” *Water Resources Research* 35:1143-1154.

Compo, G. P., J. S.Whitaker, P. D. Sardeshmukh, N. Matsui, R. J. Allan, X. Yin, B. E. Gleason, Jr., R. S. Vose, G. Rutledge, P. Bessemoulin, S. Bronnimann, M. Brunet, R. I. Crouthamel, A. N. Grant, P. Y. Groisman, P. D. Jones, M. C. Kruk, A. C. Kruger, G. J. Marshall, M. Maugeri, H. Y. Mok, Ø. Nordli, T. F. Ross, R. M. Trigo, X. L. Wang, S. D. Woodruff, and S. J.Worleyuet, 2011. “The Twentieth Century Reanalysis Project." *Quarterly Journal of the Royal Meteorological Society* 137:1–28, doi:10.1002/qj.776.

Daly, C.D., Halbleib, M., J.L. Smith, W.P. Gibson, M.K. Doggett, G.H. Taylor, J. Curtis, J., and P.P. Pasteris, 2008, “Physiographically sensitive mapping of climatological temperature and precipitation across the conterminous United States.” International Journal of Climatology, 28: 2031–2064.

Falcone, J.A., D.M. Carlisle, D.M. Wolock, and M.R. Meador. 2010. “GAGES: A Stream Gage Database for Evaluating Natural and Altered Flow Conditions in the Conterminous United States.” *Ecology* 91 (2) p. 621, a data paper in Ecological Archives E091–045–D1.

Frans, C., E. Istanbulluoglu, V. Mishra, F. Munoz-Arriola, and D.P. Lettenmaier. 2013. “Are Climatic or Land Cover Changes the Dominant Cause of Runoff Trends in the Upper Mississippi River Basin?” *Geophysical Research Letters* 40:1-7, doi:10.1002/grl.50262.

Goolsby, D.A., W.A. Battaglin, G.B. Lawrence, R.S. Artz, B.T. Aulenbach, R.P. Hooper, D.R. Keeney, and G.J. Stensland. 1999. “Flux and Sources of Nutrients in the Mississippi–Atchafalaya River Basin: Topic 3 Report for the Integrated Assessment on Hypoxia in the Gulf of Mexico.” *NOAA Coastal Ocean Program Decision Analysis Series No. 17*, NOAA Coastal Ocean Program, Silver Spring, MD. 130 p.

Helsel, D.R., and R.M. Hirsch, 1992. “Statistical Methods in Water Resources.” Elsevier, New York, 522 p.

Massei, N., B. Laignel E. Rosero A. Motelay-Massei J. Deloffre Z.-L. Yang, and A. Rossi, 2011. “A Wavelet Approach to the Short-Term to Pluri-Decennial Variability of Streamflow in the Mississippi River Basin from 1934 to 1998.” *International Journal of Climatology* 31:31–43.

McCabe, G. J., and D. M. Wolock, 2002. “A Step Increase in Streamflow in the Conterminous United States.” *Geophysical Research Letters* 29 (24): 2185, doi:10.1029/2002GL015999.

McCabe, G.J., and D.M. Wolock, 2008. “Joint Variability of Global Runoff and Global Sea-Surface Temperatures.” *Journal of Hydrometeorology* 9:816-824.

McCabe, G.J., and D.M. Wolock, 2011. “Independent Effects of Temperature and Precipitation on Modeled Runoff in the Conterminous United States.” *Water Resources Research* 47, doi:10.1029/2011WR010630.

McCabe, G.J., and D. M. Wolock, 2013. “Temporal and Spatial Variability of the Global Water Balance.” *Climatic Change* 120:375–387.

Milly, P.C.D., and K.A. Dunne, 2001. “Trends in Evaporation and Surface Cooling in the Mississippi River Basin.” *Geophysical Research. Letters* 28:1219-1222.

Qian, T., A, Dai, and K.E. Trenberth, 2007. “Hydroclimatic Trends in the Mississippi River Basin from 1948 to 2004.” *Journal of Climate* 20:4599-4614.

Rabalais, N.N., R.E. Turner, D. Justic, Q. Dortch, W.J. Wiseman, Jr., 1999. “Characterization of Hypoxia: Topic 1 Report for the Integrated Assessment on Hypoxia in the Gulf of Mexico”, NOAA Coastal Ocean Program Decision Analysis Series No. 15. NOAA Coastal Ocean Program, Silver Spring, Maryland, 167 p.

U.S. Department of Agriculture, 1991. "State Soil Geographic (STATSGO) Data Base—Date use information." Natural Resources Conservation Service Miscellaneous Publication number 1492, 110 p.

Wise, E.K., C.A. Woodhouse, G.J. McCabe, G.T. Pederson, and J.-M. St.-Jacques, 2018. "Hydroclimatology of the Missouri River Basin." *Journal of Hydrometeorology* 19:161-182, doi:10.1175/JHM-D-17-0155.1.

Wolock, D.M., and G.J. McCabe, 2018. "Water Balance Model Inputs and Outputs for the Conterminous United States, 1900-2015." *U.S. Geological Survey data release*, https://doi.org/10.5066/F71V5CWN.

TABLES

TABLE 1. Mean annual precipitation (P), potential evapotranspiration (PET), actual evapotranspiration (AET), and runoff (R) in millimeters, P-PET in millimeters, and ratios of PET/P, AET/P, R/P, AET/PET, and percent contributing area (%Area) for the 9 sub-regions identified through cluster analysis of water-year R for 8-digit hydrologic units (values are rounded to whole millimeters).

Sub-region	P	PET	AET	R	P-PET	PET/P	AET/P	R/P	AET/PET	%Area
1	415	561	351	64	-146	1.35	0.85	0.15	0.63	15
2	433	610	396	37	-177	1.41	0.91	0.09	0.65	11
3	643	616	531	112	27	0.96	0.83	0.17	0.86	8
4	475	772	445	31	-297	1.63	0.94	0.07	0.58	10
5	774	737	631	143	37	0.95	0.82	0.18	0.86	18
6	988	888	737	252	100	0.90	0.75	0.26	0.83	7
7	1248	905	782	465	343	0.73	0.63	0.37	0.86	10

8	1085	731	684	400	354	0.67	0.63	0.37	0.94	15
9	1438	943	877	561	495	0.66	0.61	0.39	0.93	6

TABLE 2. Percent of time each of the 9 sub-regions contributes the most and the least to total Mississippi River water-year runoff. The 9 sub-regions were identified through cluster analysis of water-year runoff for 8-digit hydrologic units. (Note: sums for the columns may exceed 100 percent due to rounding.)

Sub-region	Most	Least
1	0	5
2	0	60
3	0	11
4	0	22
5	2	0
6	0	3
7	19	0
8	77	0
9	2	0

LIST OF FIGURES

using a water balance model for the 9 sub-regions in the Mississippi River basin identified through cluster analysis of water-year runoff for 8-digit hydrologic units.

FIGURE 10. Percent (%) contribution to Mississippi River basin (MRB) (a) mean water-year runoff, and (b) mean monthly runoff from the 9 sub-regions in the MRB identified through cluster analysis of water-year runoff for 8-digit hydrologic units for water years 1901-2014; the line colors match the colors of the sub-regions in the inset map and the numbers by the lines indicate the sub-regions.

FIGURE 11. Mean monthly surplus (in millimeters and percent of water-year total) for the Mississippi River basin simulated using a water balance model for water years 1901-2014.

FIGURE 12. Correlations between December through May runoff (simulated using a water balance model) for the 9 sub-regions in the Mississippi River basin identified through cluster analysis of water-year runoff for 8-digit hydrologic units and mean December through May 500 hecto-Pascal heights for water years 1901-2014.

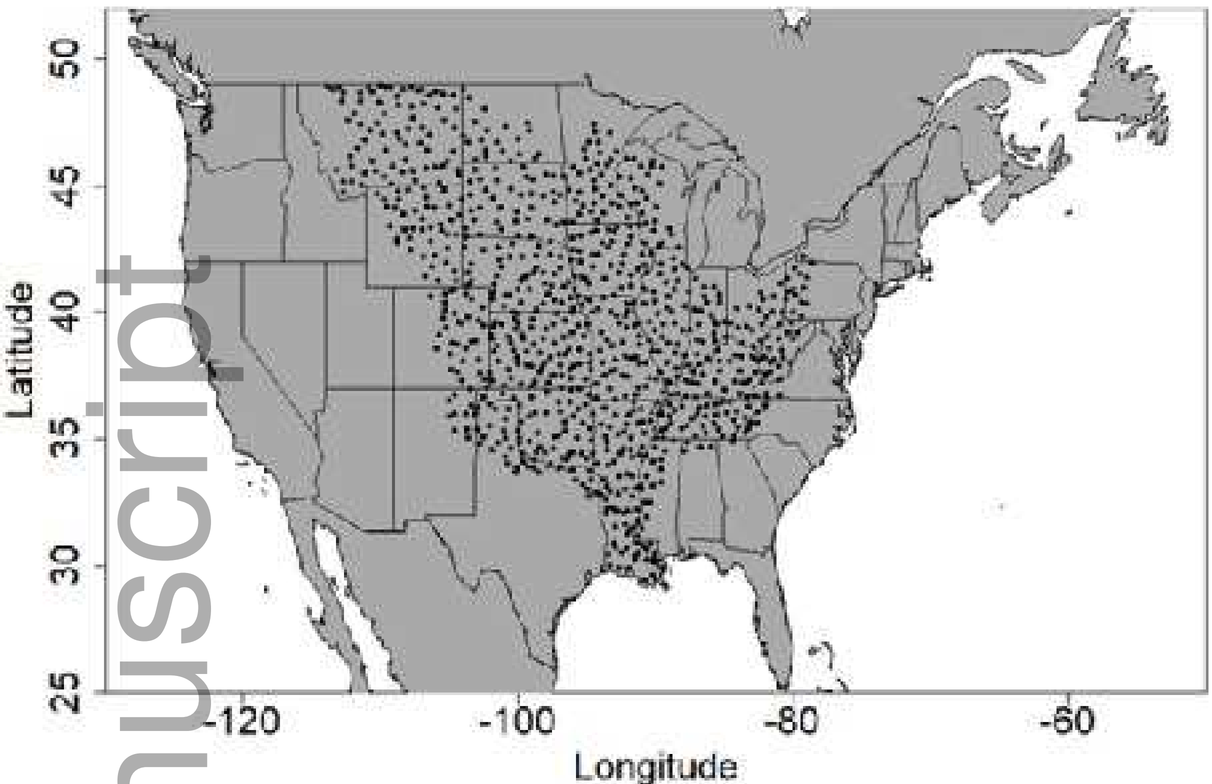

jawra_12749-18-0088_f1.tif

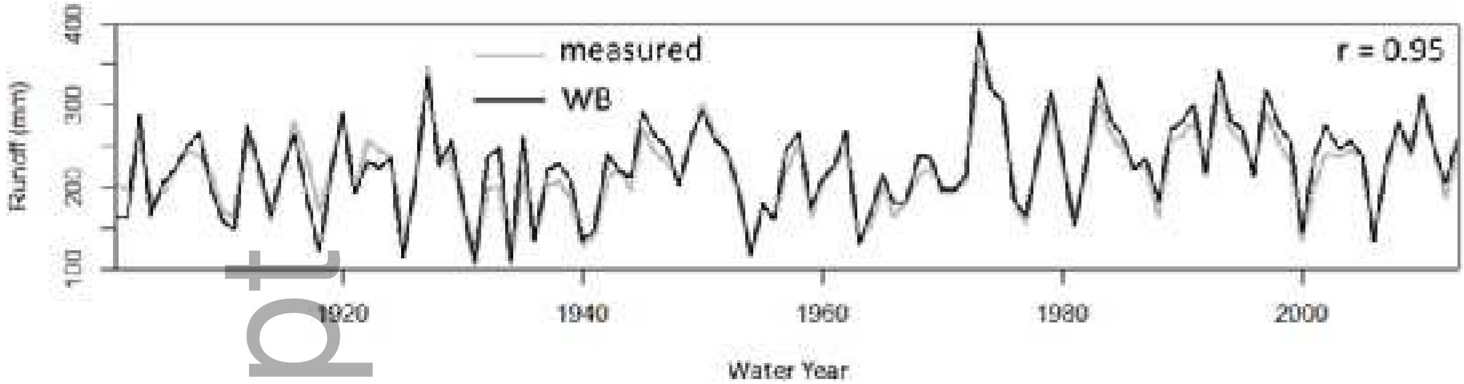

jawra_12749-18-0088_f2.tif

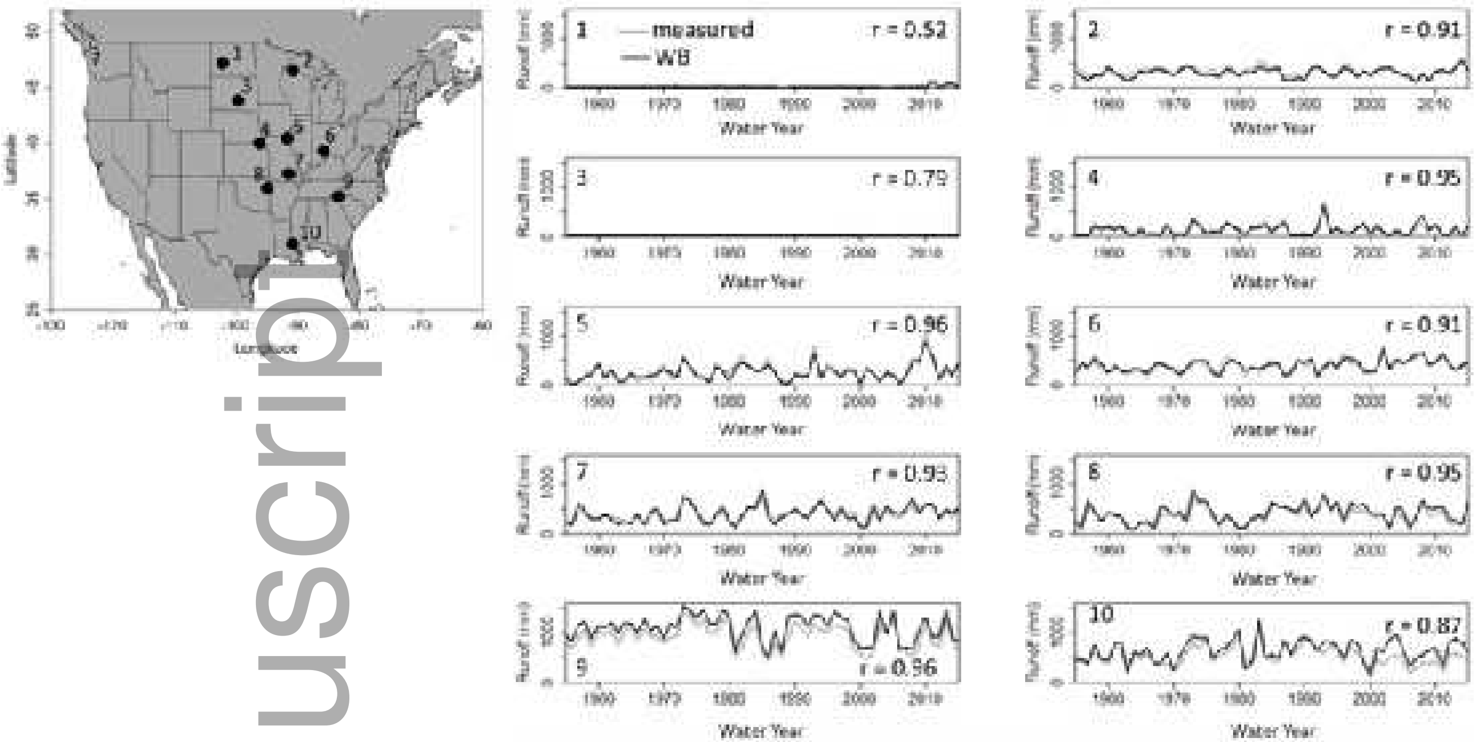

jawra_12749-18-0088_f3.tif

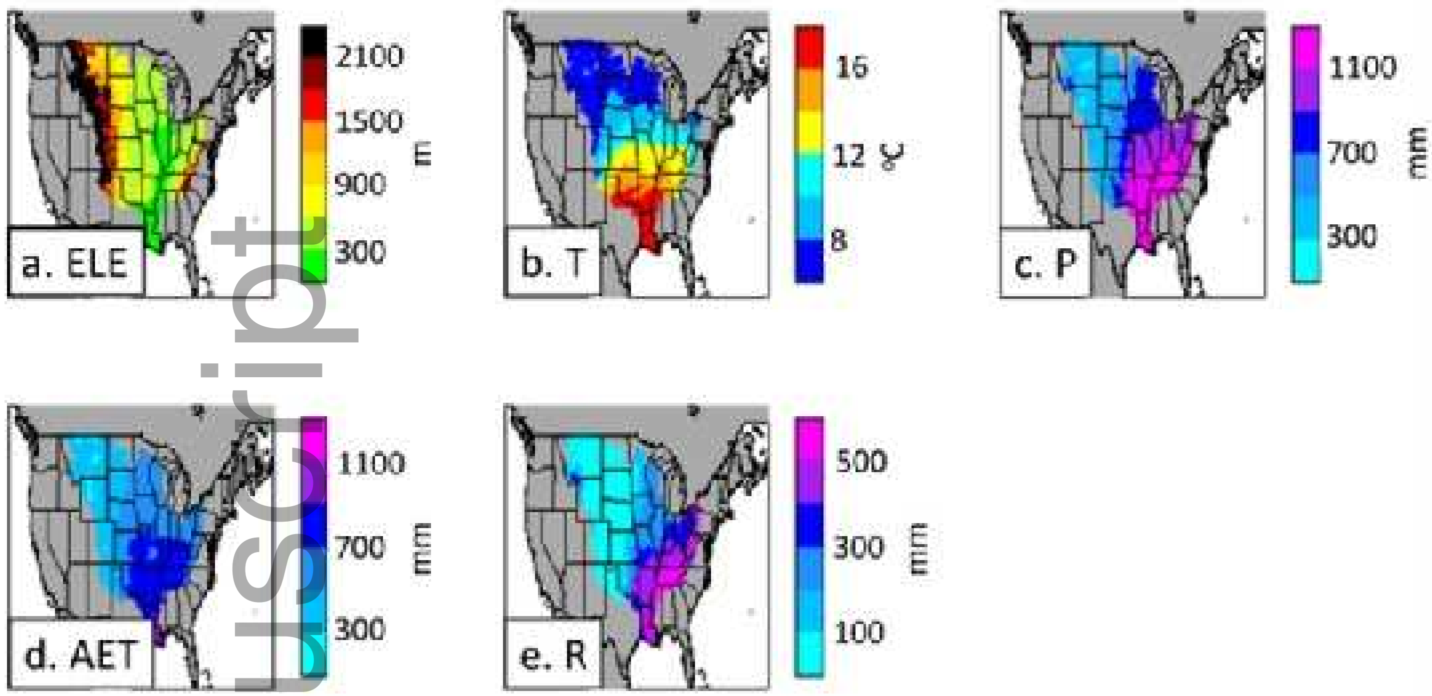

jawra_12749-18-0088_f4.tif

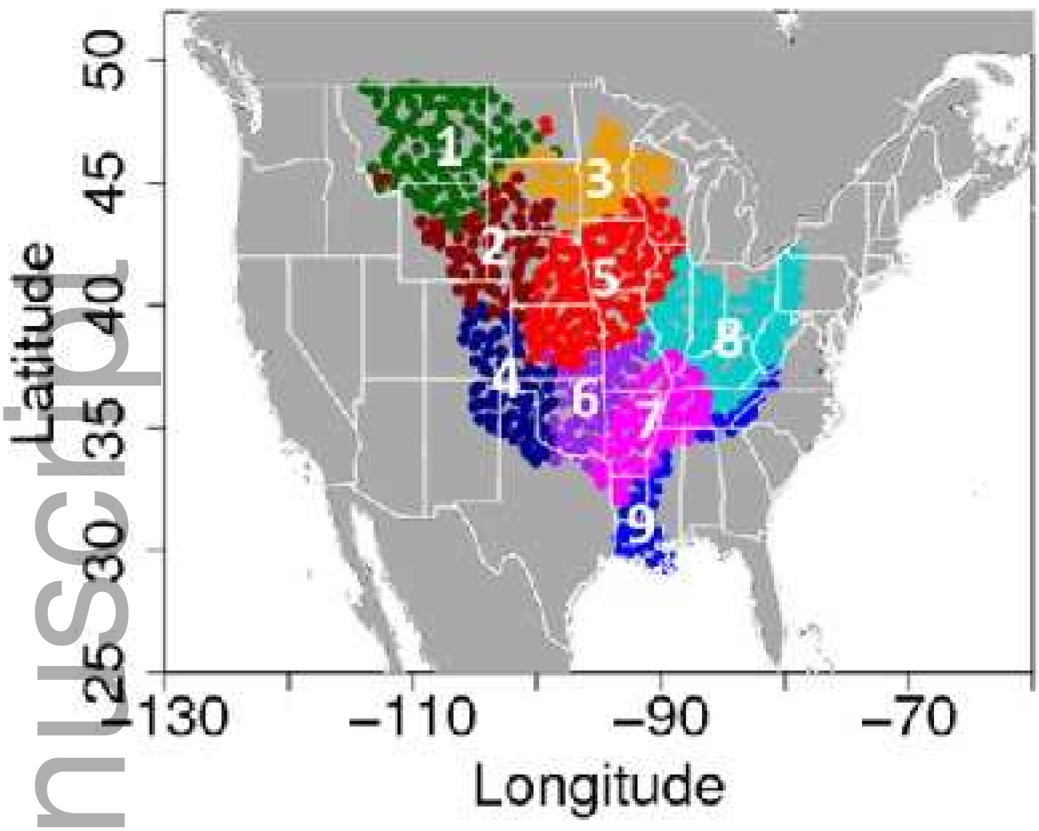

jawra_12749-18-0088_f5.tif

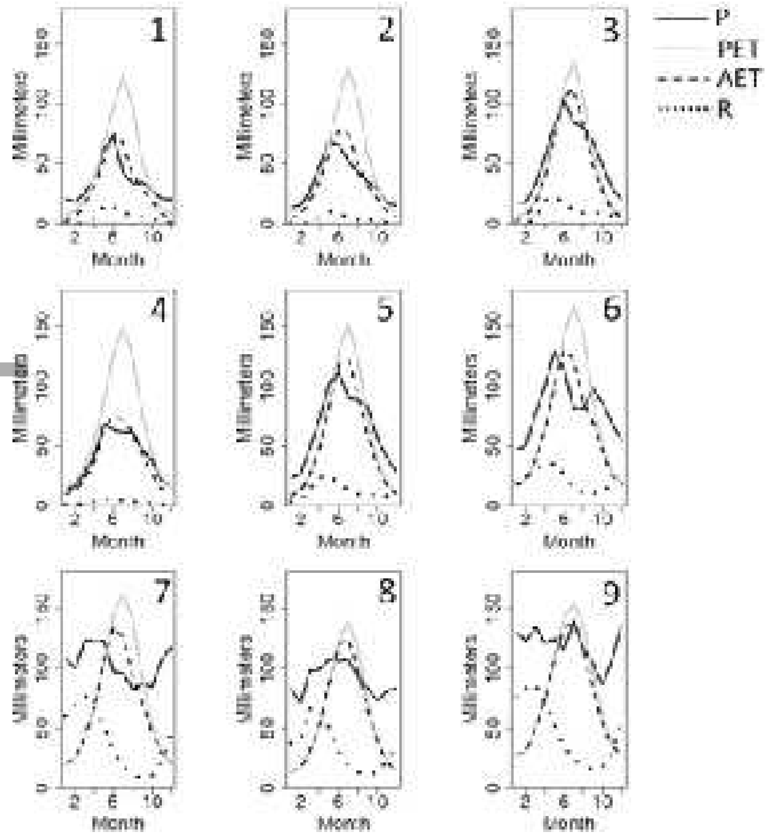

jawra_12749-18-0088_f6.tif

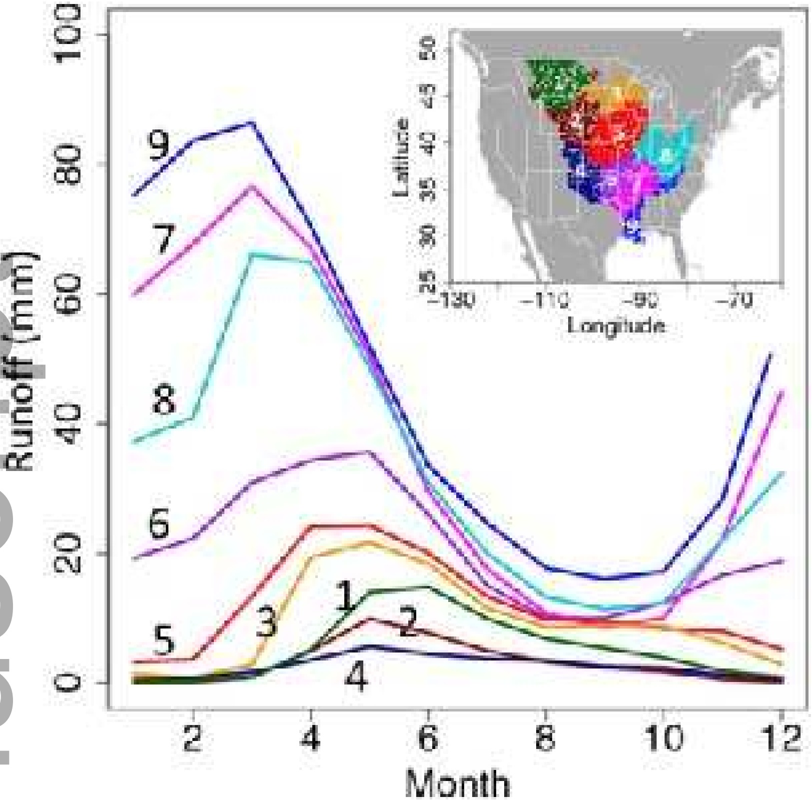

jawra_12749-18-0088_f7.tif

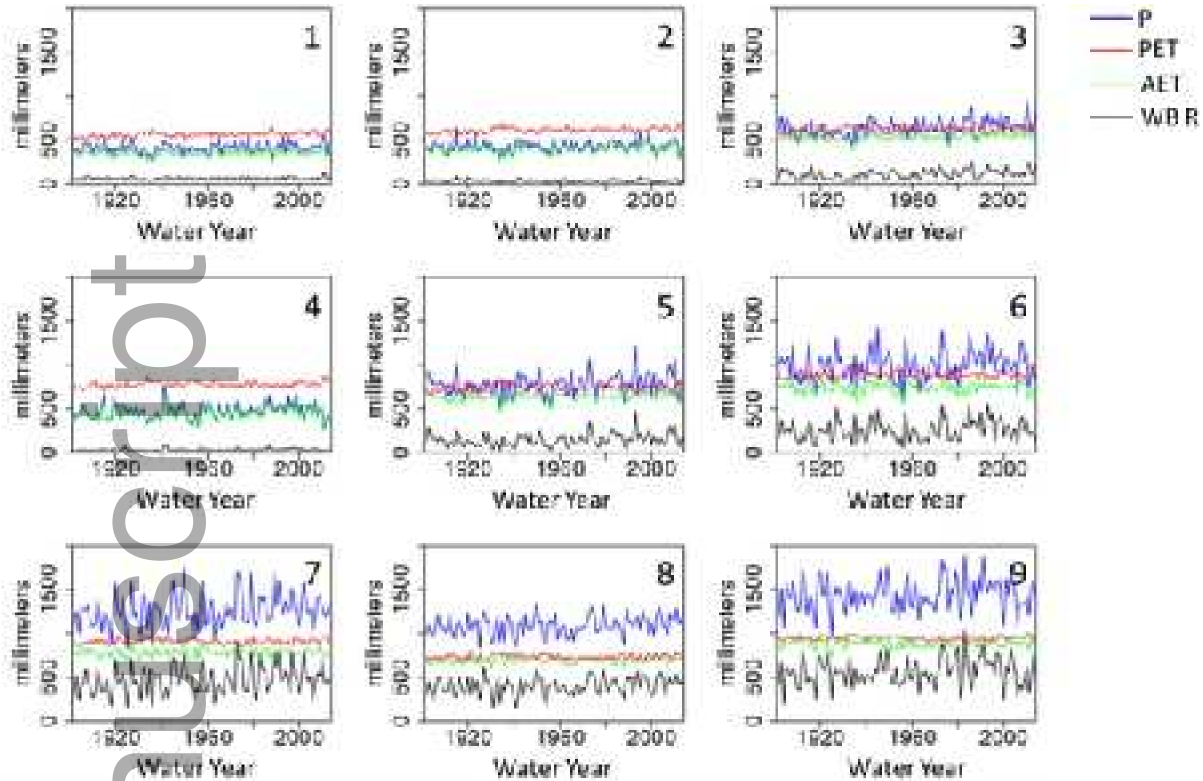

jawra_12749-18-0088_f8.tif

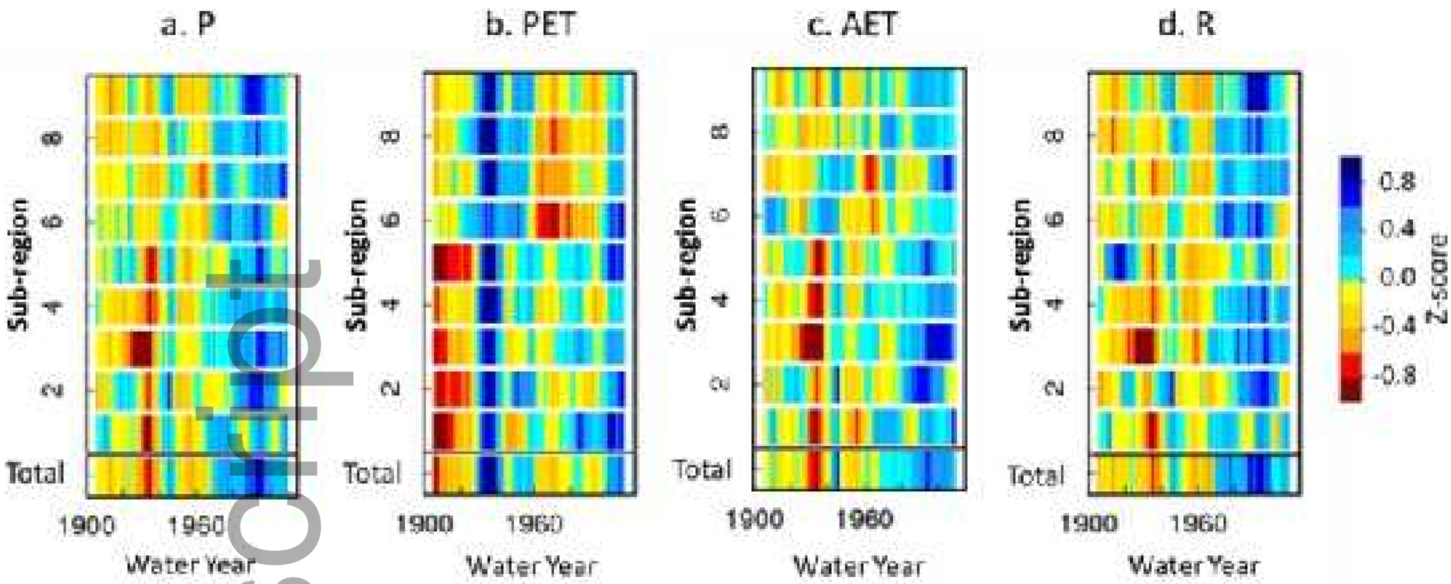

jawra_12749-18-0088_f9.tif

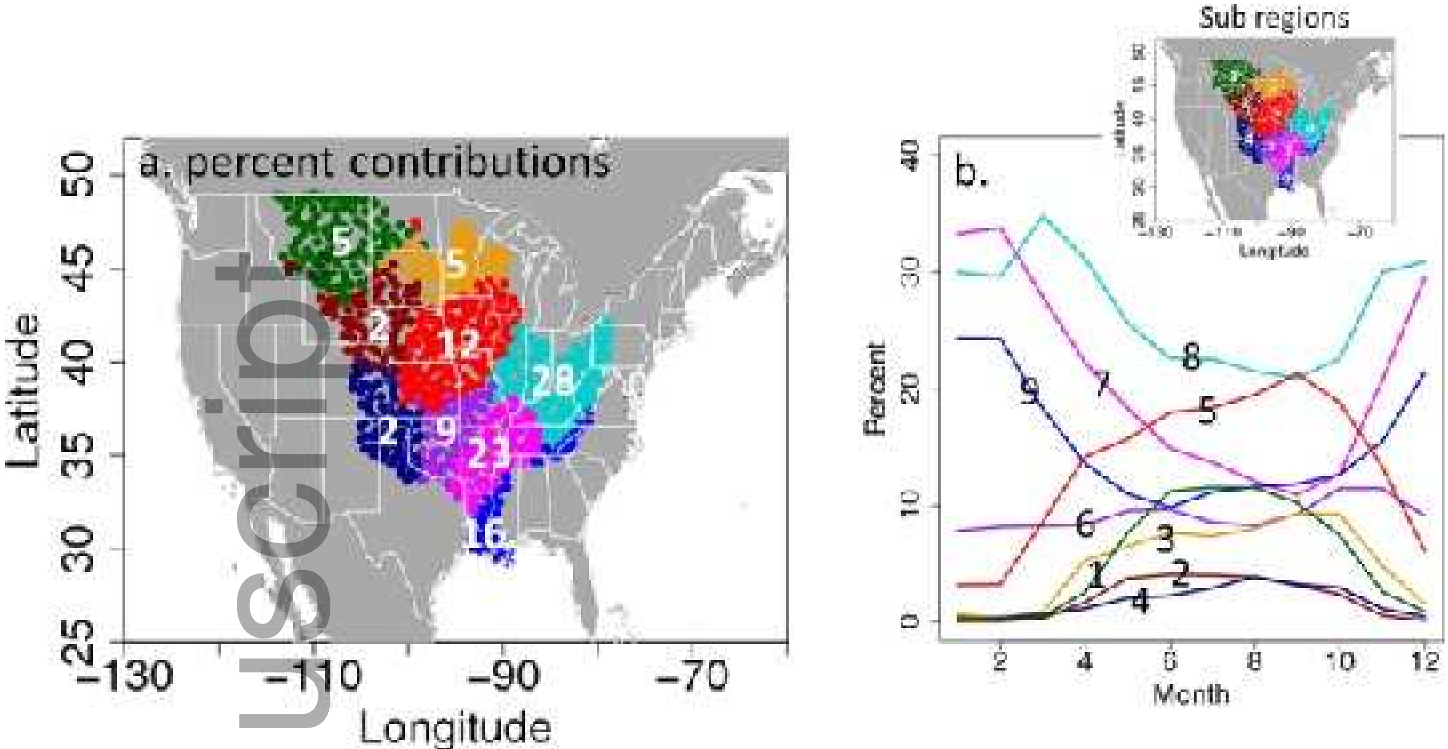

jawra_12749-18-0088_f10.tif

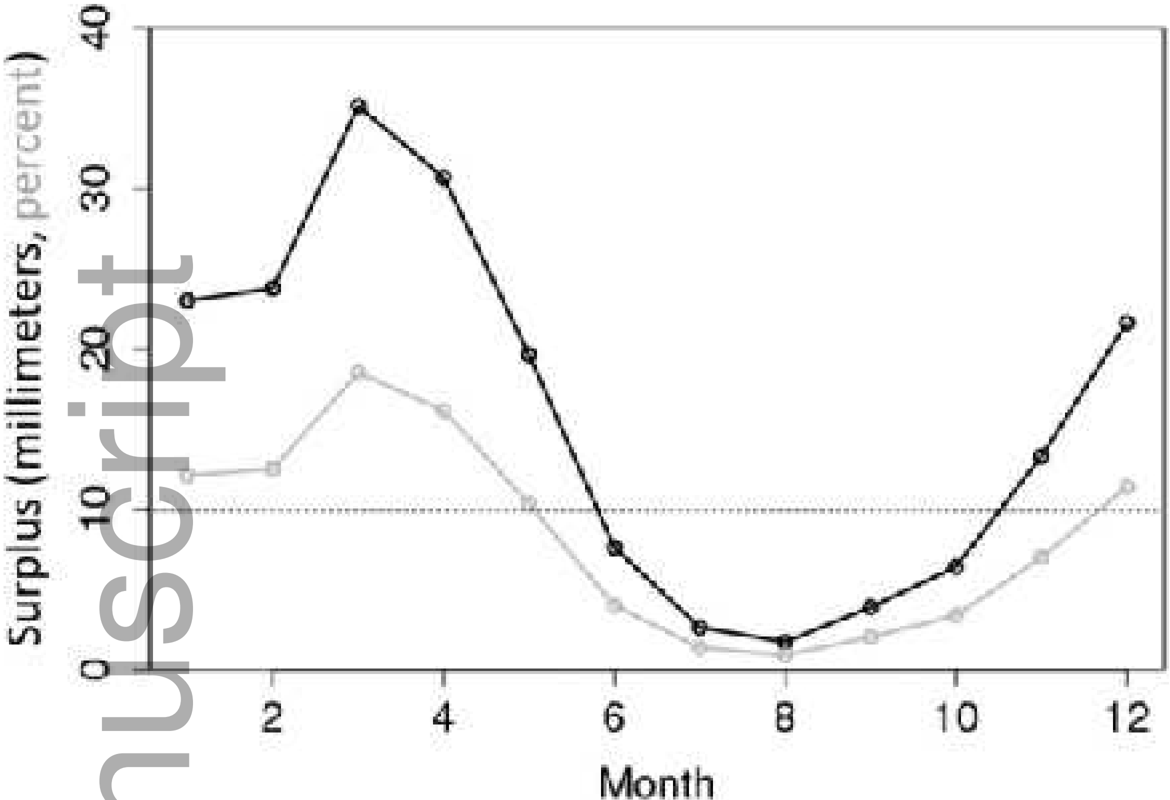

jawra_12749-18-0088_f11.tif

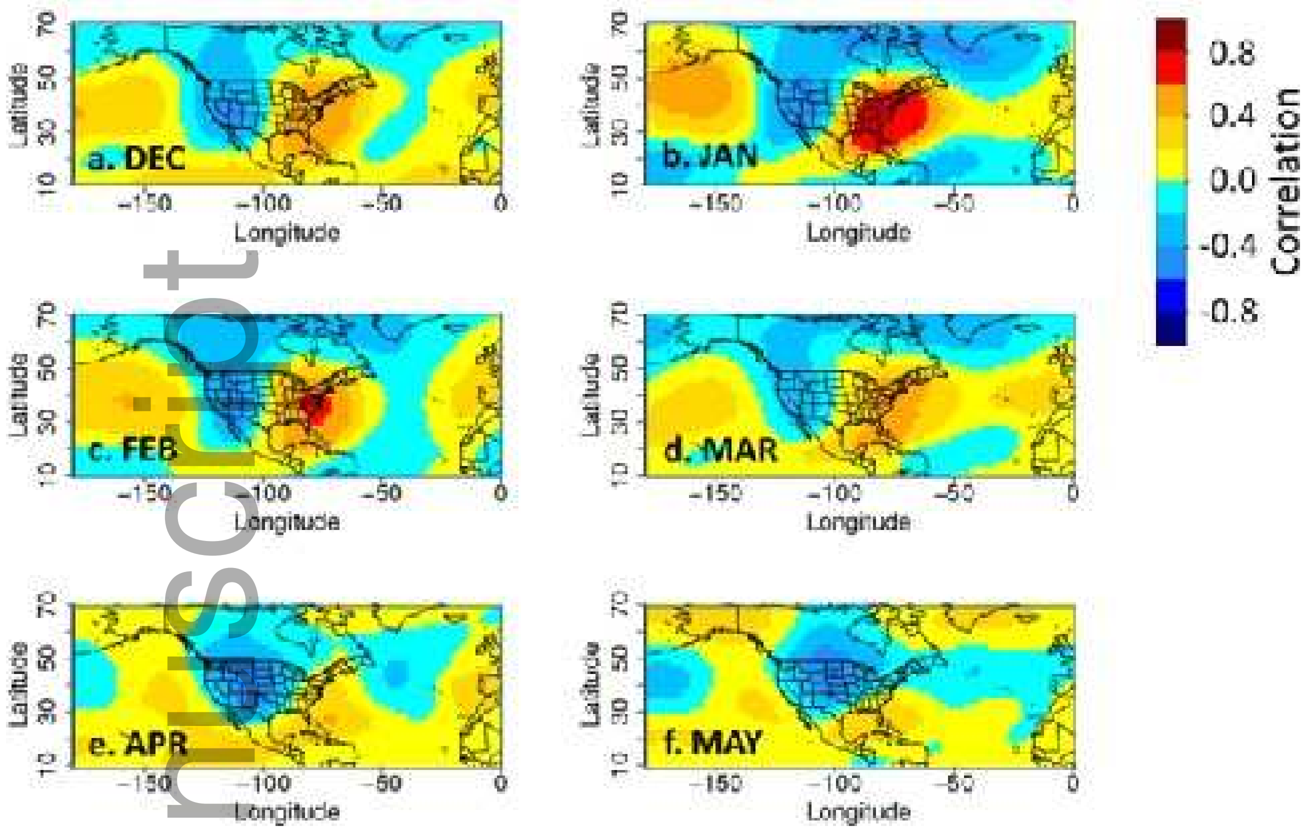

jawra_12749-18-0088_f12.tif